

EUROPEAN ORGANIZATION FOR NUCLEAR RESEARCH

CERN-PH-EP/2007-018

OPAL PR421

12th June 2007

**Search for invisibly decaying Higgs bosons
in $e^+e^- \rightarrow Z^0h^0$ production
at $\sqrt{s} = 183 - 209$ GeV**

The OPAL Collaboration

Abstract

A search is performed for Higgs bosons decaying into invisible final states, produced in association with a Z^0 boson in e^+e^- collisions at energies between 183 and 209 GeV. The search is based on data samples collected by the OPAL detector at LEP corresponding to an integrated luminosity of about 660 pb^{-1} . The analysis aims to select events containing the hadronic decay products of the Z^0 boson and large missing momentum, as expected from Higgs boson decay into a pair of stable weakly interacting neutral particles, such as the lightest neutralino in the Minimal Supersymmetric Standard Model. The same analysis is applied to a search for nearly invisible Higgs boson cascade decays into stable weakly interacting neutral particles. No excess over the expected background from Standard Model processes is observed. Limits on the production of invisibly decaying Higgs bosons produced in association with a Z^0 boson are derived. Assuming a branching ratio $\text{BR}(h^0 \rightarrow \text{invisible}) = 1$, a lower limit of 108.2 GeV is placed on the Higgs boson mass at the 95% confidence level. Limits on the production of nearly invisibly decaying Higgs bosons are also obtained.

(Submitted to Physics Letters B)

arXiv:0707.0373v1 [hep-ex] 3 Jul 2007

The OPAL Collaboration

G. Abbiendi², C. Ainsley⁵, P.F. Åkesson⁷, G. Alexander²¹, G. Anagnostou¹, K.J. Anderson⁸, S. Asai²², D. Axen²⁶, I. Bailey²⁵, E. Barberio^{7,p}, T. Barillari³¹, R.J. Barlow¹⁵, R.J. Batley⁵, P. Bechtle²⁴, T. Behnke²⁴, K.W. Bell¹⁹, P.J. Bell¹, G. Bella²¹, A. Bellerive⁶, G. Benelli⁴, S. Bethke³¹, O. Biebel³⁰, O. Boeriu⁹, P. Bock¹⁰, M. Boutemur³⁰, S. Braibant², R.M. Brown¹⁹, H.J. Burckhart⁷, S. Campana⁴, P. Capiluppi², R.K. Carnegie⁶, A.A. Carter¹², J.R. Carter⁵, C.Y. Chang¹⁶, D.G. Charlton¹, C. Ciocca², A. Csilling²⁸, M. Cuffiani², S. Dado²⁰, A. De Roeck⁷, E.A. De Wolf^{7,s}, K. Desch²⁴, B. Dienes²⁹, J. Dubbert³⁰, E. Duchovni²³, G. Duckeck³⁰, I.P. Duerdoth¹⁵, E. Etzion²¹, F. Fabbri², P. Ferrari⁷, F. Fiedler³⁰, I. Fleck⁹, M. Ford¹⁵, A. Frey⁷, P. Gagnon¹¹, J.W. Gary⁴, C. Geich-Gimbel³, G. Giacomelli², P. Giacomelli², M. Giunta⁴, J. Goldberg²⁰, E. Gross²³, J. Grunhaus²¹, M. Gruwé⁷, A. Gupta⁸, C. Hajdu²⁸, M. Hamann²⁴, G.G. Hanson⁴, A. Harel²⁰, M. Hauschild⁷, C.M. Hawkes¹, R. Hawkings⁷, G. Herten⁹, R.D. Heuer²⁴, J.C. Hill⁵, D. Horváth^{28,c}, P. Igo-Kemenes¹⁰, K. Ishii²², H. Jeremie¹⁷, P. Jovanovic¹, T.R. Junk^{6,i}, J. Kanzaki^{22,u}, D. Karlen²⁵, K. Kawagoe²², T. Kawamoto²², R.K. Keeler²⁵, R.G. Kellogg¹⁶, B.W. Kennedy¹⁹, S. Kluth³¹, T. Kobayashi²², M. Kobel^{3,t}, S. Komamiya²², T. Krämer²⁴, A. Krasznahorkay Jr.^{29,e}, P. Krieger^{6,l}, J. von Krogh¹⁰, T. Kuhl²⁴, M. Kupper²³, G.D. Lafferty¹⁵, H. Landsman²⁰, D. Lanske¹³, D. Lellouch²³, J. Letts^o, L. Levinson²³, J. Lillich⁹, S.L. Lloyd¹², F.K. Loebinger¹⁵, J. Lu^{26,b}, A. Ludwig^{3,t}, J. Ludwig⁹, W. Mader^{3,t}, S. Marcellini², A.J. Martin¹², T. Mashimo²², P. Mättig^m, J. McKenna²⁶, R.A. McPherson²⁵, F. Meijers⁷, W. Menges²⁴, F.S. Merritt⁸, H. Mes^{6,a}, N. Meyer²⁴, A. Michelini², S. Mihara²², G. Mikenberg²³, D.J. Miller¹⁴, W. Mohr⁹, T. Mori²², A. Mutter⁹, K. Nagai¹², I. Nakamura^{22,v}, H. Nanjo²², H.A. Neal³², S.W. O’Neale^{1,*}, A. Oh⁷, M.J. Oreglia⁸, S. Orito^{22,*}, C. Pahl³¹, G. Pásztor^{4,g}, J.R. Pater¹⁵, J.E. Pilcher⁸, J. Pinfold²⁷, D.E. Plane⁷, O. Pooth¹³, M. Przybycien^{7,n}, A. Quadt³¹, K. Rabbertz^{7,r}, C. Rembser⁷, P. Renkel²³, J.M. Roney²⁵, A.M. Rossi², Y. Rozen²⁰, K. Runge⁹, K. Sachs⁶, T. Saeki²², E.K.G. Sarkisyan^{7,j}, A.D. Schaile³⁰, O. Schaile³⁰, P. Scharff-Hansen⁷, J. Schieck³¹, T. Schörner-Sadenius^{7,z}, M. Schröder⁷, M. Schumacher³, R. Seuster^{13,f}, T.G. Shears^{7,h}, B.C. Shen⁴, P. Sherwood¹⁴, A. Skuja¹⁶, A.M. Smith⁷, R. Sobie²⁵, S. Söldner-Rembold¹⁵, F. Spano^{8,x}, A. Stahl¹³, D. Strom¹⁸, R. Ströhmer³⁰, S. Tarem²⁰, M. Tasevsky^{7,d}, R. Teuscher⁸, M.A. Thomson⁵, E. Torrence¹⁸, D. Toya²², I. Trigger^{7,w}, Z. Trócsányi^{29,e}, E. Tsur²¹, M.F. Turner-Watson¹, I. Ueda²², B. Ujvári^{29,e}, C.F. Vollmer³⁰, P. Vannerem⁹, R. Vértesi^{29,e}, M. Verzocchi¹⁶, H. Voss^{7,q}, J. Vossebeld^{7,h}, C.P. Ward⁵, D.R. Ward⁵, P.M. Watkins¹, A.T. Watson¹, N.K. Watson¹, P.S. Wells⁷, T. Wengler⁷, N. Wormes³, G.W. Wilson^{15,k}, J.A. Wilson¹, G. Wolf²³, T.R. Wyatt¹⁵, S. Yamashita²², D. Zer-Zion⁴, L. Zivkovic²⁰

¹School of Physics and Astronomy, University of Birmingham, Birmingham B15 2TT, UK

²Dipartimento di Fisica dell’ Università di Bologna and INFN, I-40126 Bologna, Italy

³Physikalisches Institut, Universität Bonn, D-53115 Bonn, Germany

⁴Department of Physics, University of California, Riverside CA 92521, USA

⁵Cavendish Laboratory, Cambridge CB3 0HE, UK

⁶Ottawa-Carleton Institute for Physics, Department of Physics, Carleton University, Ottawa, Ontario K1S 5B6, Canada

- ⁷CERN, European Organisation for Nuclear Research, CH-1211 Geneva 23, Switzerland
- ⁸Enrico Fermi Institute and Department of Physics, University of Chicago, Chicago IL 60637, USA
- ⁹Fakultät für Physik, Albert-Ludwigs-Universität Freiburg, D-79104 Freiburg, Germany
- ¹⁰Physikalisches Institut, Universität Heidelberg, D-69120 Heidelberg, Germany
- ¹¹Indiana University, Department of Physics, Bloomington IN 47405, USA
- ¹²Queen Mary and Westfield College, University of London, London E1 4NS, UK
- ¹³Technische Hochschule Aachen, III Physikalisches Institut, Sommerfeldstrasse 26-28, D-52056 Aachen, Germany
- ¹⁴University College London, London WC1E 6BT, UK
- ¹⁵School of Physics and Astronomy, Schuster Laboratory, The University of Manchester M13 9PL, UK
- ¹⁶Department of Physics, University of Maryland, College Park, MD 20742, USA
- ¹⁷Laboratoire de Physique Nucléaire, Université de Montréal, Montréal, Québec H3C 3J7, Canada
- ¹⁸University of Oregon, Department of Physics, Eugene OR 97403, USA
- ¹⁹Rutherford Appleton Laboratory, Chilton, Didcot, Oxfordshire OX11 0QX, UK
- ²⁰Department of Physics, Technion-Israel Institute of Technology, Haifa 32000, Israel
- ²¹Department of Physics and Astronomy, Tel Aviv University, Tel Aviv 69978, Israel
- ²²International Centre for Elementary Particle Physics and Department of Physics, University of Tokyo, Tokyo 113-0033, and Kobe University, Kobe 657-8501, Japan
- ²³Particle Physics Department, Weizmann Institute of Science, Rehovot 76100, Israel
- ²⁴Universität Hamburg/DESY, Institut für Experimentalphysik, Notkestrasse 85, D-22607 Hamburg, Germany
- ²⁵University of Victoria, Department of Physics, P O Box 3055, Victoria BC V8W 3P6, Canada
- ²⁶University of British Columbia, Department of Physics, Vancouver BC V6T 1Z1, Canada
- ²⁷University of Alberta, Department of Physics, Edmonton AB T6G 2J1, Canada
- ²⁸Research Institute for Particle and Nuclear Physics, H-1525 Budapest, P O Box 49, Hungary
- ²⁹Institute of Nuclear Research, H-4001 Debrecen, P O Box 51, Hungary
- ³⁰Ludwig-Maximilians-Universität München, Sektion Physik, Am Coulombwall 1, D-85748 Garching, Germany
- ³¹Max-Planck-Institute für Physik, Föhringer Ring 6, D-80805 München, Germany
- ³²Yale University, Department of Physics, New Haven, CT 06520, USA

^a and at TRIUMF, Vancouver, Canada V6T 2A3

^b now at University of Alberta

^c and Institute of Nuclear Research, Debrecen, Hungary

^d now at Institute of Physics, Academy of Sciences of the Czech Republic 18221 Prague, Czech Republic

^e and Department of Experimental Physics, University of Debrecen, Hungary

^f and MPI München

^g and Research Institute for Particle and Nuclear Physics, Budapest, Hungary

^h now at University of Liverpool, Dept of Physics, Liverpool L69 3BX, U.K.

ⁱ now at Dept. Physics, University of Illinois at Urbana-Champaign, U.S.A.

- ^j and The University of Manchester, M13 9PL, United Kingdom
^k now at University of Kansas, Dept of Physics and Astronomy, Lawrence, KS 66045, U.S.A.
^l now at University of Toronto, Dept of Physics, Toronto, Canada
^m current address Bergische Universität, Wuppertal, Germany
ⁿ now at University of Mining and Metallurgy, Cracow, Poland
^o now at University of California, San Diego, U.S.A.
^p now at The University of Melbourne, Victoria, Australia
^q now at IPHE Université de Lausanne, CH-1015 Lausanne, Switzerland
^r now at IEKP Universität Karlsruhe, Germany
^s now at University of Antwerpen, Physics Department, B-2610 Antwerpen, Belgium; supported by Interuniversity Attraction Poles Programme – Belgian Science Policy
^t now at Technische Universität, Dresden, Germany
^u and High Energy Accelerator Research Organisation (KEK), Tsukuba, Ibaraki, Japan
^v now at University of Pennsylvania, Philadelphia, Pennsylvania, USA
^w now at TRIUMF, Vancouver, Canada
^x now at Columbia University
^y now at CERN
^z now at DESY
* Deceased

1 Introduction

The Higgs boson [1] is required by the Standard Model (SM) [2] but has not yet been observed [3]. At LEP II energies it should be produced mainly through the “Higgs-strahlung” process ($e^+e^- \rightarrow Z^* \rightarrow H^0 Z^0$) if its mass is sufficiently low. In the SM, the Higgs boson dominantly decays into a pair of the heaviest kinematically accessible particles, which would be a b-quark pair at LEP II. In some models beyond the SM, however, the Higgs boson can decay predominantly into a pair of invisible particles if the process is kinematically allowed.

The Minimal Supersymmetric Standard Model (MSSM) [4] is one of the models which allows for invisibly decaying Higgs bosons [5], through the $h^0 \rightarrow \tilde{\chi}_1^0 \tilde{\chi}_1^0$ process, where $\tilde{\chi}_1^0$ is the lightest neutralino, if the mass of $\tilde{\chi}_1^0$ is lighter than half of the Higgs mass and R-parity is conserved. If $\tilde{\chi}_1^0$ is purely photino-like, the decay $h^0 \rightarrow \tilde{\chi}_1^0 \tilde{\chi}_1^0$ is suppressed. In this case a decay $h^0 \rightarrow \tilde{\chi}_1^0 \tilde{\chi}_2^0$, where $\tilde{\chi}_2^0$ is the second lightest neutralino, becomes dominant if it is allowed kinematically. If the mass difference (ΔM) between $\tilde{\chi}_2^0$ and $\tilde{\chi}_1^0$ is small, the visible products of the decay $\tilde{\chi}_2^0 \rightarrow \tilde{\chi}_1^0 Z^*/\gamma$ are soft and the event topology is similar to that produced by an invisible Higgs decay $h^0 \rightarrow \tilde{\chi}_1^0 \tilde{\chi}_1^0$. The $h^0 \rightarrow \tilde{\chi}_1^0 \tilde{\chi}_2^0$ processes are therefore referred to as nearly invisible Higgs decays.

In a non-linear supersymmetric model, the Higgs boson can decay into a neutrino plus a Goldstino [6], and the invisible decay can be dominant. In other models beyond the SM with a spontaneously broken global symmetry, the Higgs boson could decay into a pair of massless

Goldstone bosons, called Majorons [7], which couple strongly to the Higgs boson. In models with extra dimensions, the Higgs boson can decay into a neutrino pair [8] or can oscillate into invisible states if the Higgs boson mixes with a graviscalar [9] which is a scalar graviton and escapes in the extra dimension. Models which introduce hidden scalar sectors which couple to the Higgs sector can also cause invisible decays of the Higgs boson [10].

In this paper, a search for invisibly decaying Higgs bosons ($h^0 \rightarrow \chi^0 \chi^0$)^a is presented using the data collected at various centre-of-mass energies (\sqrt{s}) between 183 and 209 GeV by the OPAL detector at LEP, corresponding to an integrated luminosity of 659.3 pb⁻¹. The topology of events containing invisibly decaying Higgs bosons produced through the process $e^+e^- \rightarrow h^0 Z^0$ is characterised by the decay products of the associated Z^0 boson plus large missing momentum and a visible mass (M_{vis}) of the event consistent with m_{Z^0} . Here it is also assumed that the decay width of the Higgs boson is negligibly small. A search for invisibly decaying Higgs bosons with large decay width is presented in Ref. [11]. The search presented here looks for a hadronic decay of the Z^0 boson in association with missing energy. To cover other Z^0 decay modes, the results from this search are combined with the results of the decay-mode independent $h^0 Z^0$ search [12] where the Z^0 decays into e^+e^- or $\mu^+\mu^-$. The results of the invisibly decaying Higgs boson search at LEP I [13] are also included to enhance the sensitivities to lower Higgs boson masses.

The same analysis is applied to search for the production of nearly invisibly decaying Higgs bosons: $e^+e^- \rightarrow Z^0 h^0 \rightarrow (q\bar{q})(\chi^0 \chi^0)$ assuming a small mass difference $\Delta M = 2$ and 4 GeV between χ^0 and χ^0 . The standard neutralino searches [14] are sensitive to cases with $\Delta M \geq 3$ GeV. Similar searches for an invisibly decaying Higgs boson have been carried out by the other LEP experiments [15].

2 The OPAL Detector, Data and Event Simulation

2.1 The OPAL Detector

The OPAL detector is described in detail in Ref. [16]. The central tracking system consisted of a silicon micro-vertex detector, a vertex drift chamber, a jet chamber and z -chambers. In the range $|\cos\theta| < 0.73$, 159 points could be measured in the jet chamber along each track^b. At least 20 points on a track could be obtained over 96% of the full solid angle. The whole tracking system was located inside a 0.435 T axial magnetic field. A lead-glass electromagnetic calorimeter (ECAL) providing acceptance within $|\cos\theta| < 0.984$, together with pre-samplers and time-of-flight scintillators, was located outside the magnet coil in the barrel region and at the front end of each endcap. The magnet return yoke was instrumented for hadron calorimetry

^aWhile motivated by the lightest neutralino of the MSSM, throughout this paper we use χ^0 as a generic symbol for a neutral weakly interacting massive particle resulting from an invisible Higgs boson decay.

^bA right-handed coordinate system is adopted, where the x -axis points to the centre of the LEP ring, and positive z is along the electron beam direction. The angles θ and ϕ are the polar and azimuthal angles, respectively.

(HCAL), giving a polar angle coverage of $|\cos\theta| < 0.99$, and was surrounded by external muon chambers. The forward detectors (FD) and silicon-tungsten calorimeters (SW) located on both sides of the interaction point measured the luminosity and complete the geometrical acceptance down to 24 mrad in polar angle. The small gap between the endcap ECAL and FD was filled by an additional electromagnetic calorimeter, called the gamma-catcher (GC), and a counter consisting of tile scintillators called the MIP plug.

2.2 Data and event simulation

The search is performed using the OPAL data collected at \sqrt{s} between 183 and 209 GeV with an integrated luminosity of 659.3 pb^{-1} . The integrated luminosities at each \sqrt{s} are listed in Table 1.

Nominal \sqrt{s} (GeV)	183	189	192	196	200	202	204	205	206	208
$\langle\sqrt{s}\rangle$ (GeV)	182.7	188.6	191.6	195.5	199.5	201.7	203.7	205.0	206.5	208.0
Lumi. (pb^{-1})	56.1	178.2	29.0	71.7	74.9	39.3	6.3	71.4	124.6	7.8

Table 1: Average centre-of-mass energies ($\langle\sqrt{s}\rangle$) and integrated luminosities collected at each nominal centre-of-mass energy after detector status cuts. The uncertainty on the luminosity measurement is 0.5%.

The signal detection efficiencies and expected number of background events are estimated using a variety of Monte Carlo (MC) samples. Signal samples of invisibly decaying and nearly invisibly decaying Higgs boson processes are produced using the HZHA generator [17]. The Higgs bosons are produced in association with a Z^0 boson, and then are forced to decay into a pair of invisible particles. Samples of $h^0 \rightarrow \chi^0 \chi^0$ at each \sqrt{s} are produced in one GeV steps in the Higgs boson mass range from 1 to 120 GeV with 2000 events per mass point. The $h^0 \rightarrow \chi^0 \chi^{0'}$ samples are generated with mass differences ΔM of 2 and 4 GeV at 5 or 10 GeV Higgs boson mass intervals between 30 and 120 GeV, with 500 or 1000 events per point. The detection efficiencies are determined at fixed values of the Higgs boson mass using the above samples and then interpolated to arbitrary masses with a spline fit.

The most important background processes are $e^+e^- \rightarrow W^+W^- \rightarrow \ell\nu q\bar{q}$ and $e^+e^- \rightarrow Z^0Z^0 \rightarrow \nu\bar{\nu}q\bar{q}$. The first of these channels fakes a signal when the lepton is within a jet or escapes detection along the beam axis, and the second is an irreducible background for Higgs bosons with masses in the vicinity of the Z^0 boson mass. The radiative multihadron process $e^+e^- \rightarrow q\bar{q}(\gamma)$ also contributes due to the escape of photon into the beam pipe.

The background processes are simulated primarily by the following event generators. For two-fermion (2f) final states, events are generated by PYTHIA [18] and KK2f [19] ($q\bar{q}(\gamma)$), BH-WIDE [22] and TEEGG [23] ($e^+e^-(\gamma)$), and KORALZ [24] and KK2f ($\mu^+\mu^-(\gamma)$ and $\tau^+\tau^-(\gamma)$), for four-fermion (4f) final states, by grc4f [20] (4f processes with final states of $e^+e^-f\bar{f}$) and KORALW [21] (4f processes except final states with $e^+e^-f\bar{f}$), and for so-called two-photon processes where the initial-state electron and positron radiate photons which interact to produce

additional final state fermions, by PHOJET [25], PYTHIA and Vermaseren [26] (hadronic and leptonic two-photon processes; $e^+e^-q\bar{q}$ and $e^+e^-\ell^+\ell^-$). The generated partons are hadronised using JETSET [18] with parameters described in Ref. [27]. The resulting particles are processed through a full simulation [28] of the OPAL detector.

3 Selection criteria

The search criteria are optimised at each \sqrt{s} using the MC samples with 10 mass points just below the kinematic limit for the invisibly decaying Higgs, $h^0 \rightarrow \chi^0\chi^0$. For the $h^0 \rightarrow \chi^0\chi^{0'}$ final state, the decay products of the Z^0 may be accompanied by a soft jet with small visible mass and energy, aligned in the direction of the missing momentum. Since the two event topologies are very similar, the selection criteria for the $h^0 \rightarrow \chi^0\chi^0$ are also applied to the $h^0 \rightarrow \chi^0\chi^{0'}$ final states. The analysis begins with a preselection to ensure data quality, followed by a combination of cut-based and likelihood-based analysis.

Experimental variables are calculated using the four-momenta of charged particle tracks, and ECAL and HCAL clusters. The clusters associated with tracks are also used in the energy and momentum calculations, after subtracting the momenta of tracks from the energy observed in the calorimeters to reduce double counting of energy [29].

3.1 Preselection

The following requirements are applied to reduce beam-related background as well as two-photon events:

- (P1) The event must not contain any charged particle track or ECAL cluster with reconstructed energy greater than $1.3 \times E_{\text{beam}}$, where E_{beam} is the beam energy.
- (P2) $E_{\text{vis}}^{|\cos\theta|>0.9} / E_{\text{vis}} < 0.2$, where E_{vis} is the total visible energy and $E_{\text{vis}}^{|\cos\theta|>0.9}$ is the visible energy in the region defined by $|\cos\theta| > 0.9$.
- (P3) $N_{\text{ch}}^{\text{good}} / N_{\text{ch}} > 0.2$, where $N_{\text{ch}}^{\text{good}}$ and N_{ch} are the number of good charged particle tracks defined as in Ref. [30] and total number of tracks, respectively.
- (P4) $M_{\text{vis}} > 3 \text{ GeV}$, where M_{vis} is the invariant mass of the event.
- (P5) $p_{\text{T}} > 1.8 \text{ GeV}$, where p_{T} is the magnitude of the vector sum of the transverse momenta of the reconstructed objects in the event with respect to the beam direction.
- (P6) Forward energy veto: events are rejected if there is more than 2/2/5 GeV deposited in either side of the forward detectors, SW/FD/GC respectively, or if there is any significant activity in the MIP plug. This forward energy veto is introduced to ensure that the data

sample consists of well-measured events. The efficiency loss due to vetoes on random detector occupancy has been studied with a sample consisting of random triggers, and was found to be between 2.2% and 4.1%, depending on \sqrt{s} . The signal detection efficiencies and the numbers of expected background events are corrected for such losses.

- (P7) $N_{\text{jets}} > 1$, where N_{jets} is the number of jets reconstructed with the Durham algorithm [31] with a jet resolution parameter $y_{\text{cut}} = 0.005$. This reduces monojet-like background caused primarily by beam-gas and beam-wall interactions.
- (P8) $|\cos \theta_{\text{miss}}| < 0.95$, where θ_{miss} is the polar angle of the missing momentum of the event. The $q\bar{q}(\gamma)$ background is reduced by this requirement.
- (P9) $M_{\text{miss}}^2 > 0 \text{ GeV}^2$, where M_{miss}^2 is missing mass squared and is calculated with the visible mass scaled to the Z^0 -mass, *i.e.* $M_{\text{miss}}^2 = s - 2\sqrt{s}\frac{m_{Z^0}}{M_{\text{vis}}}E_{\text{vis}} + m_{Z^0}^2$. This formula is applied to avoid a negative M_{miss}^2 .

The number of data events remaining after these cuts and those expected from SM background processes are summarised in the first row of Table 2.

3.2 Main selection criteria

The main selection consists of a cut-based analysis followed by a likelihood-based analysis using the same technique as described in Ref. [32]. After the preselection (P1-P9) the following cuts are applied in sequence:

- (B1) $N_{\text{ch}}^{\text{good}} > 4$.
- (B2) $p_{\text{T}} > 6 \text{ GeV}$.
- (B3) $\max(|\cos \theta_{\text{jet}}|) < 0.95$, where θ_{jet} is the polar angle of the jet axis after the event is forced into two jets with the Durham algorithm. This requirement leaves events containing well measured jets.
- (B4) The number of isolated charged leptons identified as in Ref [32] is required to be zero to reduce the background contribution from semi-leptonic W^+W^- and Z^0Z^0 events.
- (B5) $120 \text{ GeV} > M_{\text{vis}} > 50 \text{ GeV}$.

The distributions of p_{T} and $\max(|\cos \theta_{\text{jet}}|)$, just before applying the respective cuts, are shown in Figure 1. The numbers of selected events, the expected background and the signal efficiencies, after each cut, are shown in Table 2.

After applying the above cuts, the selected sample is divided into two categories, namely events with two jets (“2-jet”) and with more than two jets (“>2-jet”), where the number of jets

Cut	Data	Background			Efficiency (%) $m_{h^0} = 105 \text{ GeV}$
		Total	2f	4f	
Pre	101653	86767	48277	8299	67.6
B1	40031	34158	14253	7513	67.6
B2	16895	17037	10391	6503	65.8
B3	16694	16882	10372	6379	65.3
B4	11476	11654	8855	2695	56.1
B5	1045	1069	523	532	55.5
LH 2-jet	194	$205.7 \pm 1.8 \pm 1.3$	46.1	157.1	23.7
>2-jet	278	$279.4 \pm 1.9 \pm 1.5$	44.1	233.5	23.4

Table 2: Cut flow table at $\sqrt{s} = 183\text{--}209 \text{ GeV}$. Each row shows the number of events after each cut of the selection (described in the text) for the data and the expected background. The backgrounds from two-fermion and four-fermion processes are shown separately. The contributions from two-photon processes are not shown individually but included in the total background. The background estimates are normalised to luminosity at each energy and summed. The first quoted error on background estimates is statistics and the second systematic. The last column shows the luminosity-weighted average of selection efficiencies for the $Z^0 h^0 \rightarrow (q\bar{q})(\chi^0 \chi^0)$ final state with $m_{h^0} = 105 \text{ GeV}$. The last two rows show the final numbers of selected events, expected background and the efficiency after the likelihood analysis (LH) in each category. The efficiency in a category is the fraction of signal Monte Carlo events which pass the selection requirements. The background numbers and signal efficiencies include the occupancy correction determined at each \sqrt{s} due to the forward energy veto.

is defined by the Durham algorithm with $y_{\text{cut}} = 0.005$. A likelihood analysis (LH) is built up for each category separately, with the same technique as described in Ref. [32] using the input variables:

- $\cos \theta_{\text{miss}}$
- the acoplanarity angle when the event is forced into two jets, ϕ_{acop} .
- the invariant mass of the two jets with the smallest opening angle, $M_{2\text{jets}}^{\text{min}\phi}$.
- d_{23} , which is defined as $E_{\text{vis}}^2 \times y_{23}$, where y_{23} is the jet resolution parameter at the transition point from two to three jets in the jet reconstruction.
- $\min(N_{\text{ch}}^{\text{jet}})$, which is the smallest charged multiplicity of any jet in the event.

The distributions of input variables for the expected background are different between the two categories as shown in Figure 2, due to the different contribution from background sources. The resulting likelihood distribution for each category is shown in Figure 3. The remaining background in the signal-like region is dominated by semi-leptonic 4f events.

The properties of 4f background events are similar to the signal, thus broadening the likelihood peak for the signal. The final results are obtained by requiring the likelihood to be larger than 0.2. The numbers of observed and expected events are summarised in Table 2 and Table 3. The efficiency in a category is defined as the ratio of the number of selected events in that category to the total number of produced events; the sum of efficiencies in the two categories provides the total efficiency at a given mass point. The efficiencies for the $h^0 \rightarrow \chi^0 \chi^{0'}$ processes are relatively lower than those for the $h^0 \rightarrow \chi^0 \chi^0$, as shown in Table 4.

		\sqrt{s} (GeV)									
		183	189	192	196	200	202	204	205	206	208
2-jet	Data	17	52	7	19	20	12	1	22	43	1
	Background	19.0	54.6	9.0	22.4	23.4	12.2	2.1	22.1	38.5	2.4
	Eff.(%)	17.7	20.0	21.1	22.5	27.2	26.7	28.5	27.6	27.2	29.2
>2-jet	Data	15	78	18	31	41	12	2	32	47	2
	Background	30.6	76.1	13.1	31.7	30.8	15.4	2.6	28.5	47.6	3.1
	Eff.(%)	17.5	20.9	20.7	24.3	25.0	25.1	24.9	23.6	26.1	23.6

Table 3: Number of candidate events and expected background for each category at each \sqrt{s} , together with signal efficiencies for $m_{h^0} = 105$ GeV.

The systematic errors on signal efficiencies and the numbers of expected background events are estimated using the following procedures. The uncertainty corresponding to the modelling of each selection variable is determined by comparing the mean values of the distribution of that variable between data and SM background MC samples at $\sqrt{s} = m_{Z^0}$ after applying the preselection. Efficiencies and numbers of expected background events are estimated again,

Cat.	Decay Mode	ΔM (GeV)	Efficiencies (%) at Higgs Mass(GeV)										
			10	20	30	40	50	60	70	80	90	100	105
2-jet	$\chi^0\chi^0$	—	13	16	20	22	26	27	27	27	27	25	24
	$\chi^0\chi^0\gamma$	2	—	—	11	14	18	22	24	23	25	23	24
	$\chi^0\chi^0\gamma$	4	—	—	8	11	14	17	19	20	20	20	21
	$\chi^0\chi^0Z^*$	2	—	—	9	13	16	19	22	22	23	21	22
	$\chi^0\chi^0Z^*$	4	—	—	9	13	16	18	21	22	22	21	22
>2-jet	$\chi^0\chi^0$	—	12	14	18	20	23	24	24	25	25	23	23
	$\chi^0\chi^0\gamma$	2	—	—	10	14	17	19	22	23	23	22	23
	$\chi^0\chi^0\gamma$	4	—	—	10	14	17	19	22	23	24	23	24
	$\chi^0\chi^0Z^*$	2	—	—	12	15	18	20	23	24	24	23	24
	$\chi^0\chi^0Z^*$	4	—	—	12	16	19	21	23	24	25	24	25

Table 4: *Luminosity-weighted averages of efficiency for $\chi^0\chi^0$, $\chi^0\chi^0\gamma$ and $\chi^0\chi^0Z^*$ channels. No Monte Carlo samples are available in the $\chi^0\chi^0\gamma$ and $\chi^0\chi^0Z^*$ channels for Higgs masses less than 30 GeV.*

shifting each variable separately by its uncertainty. Relative changes to the original values of efficiencies and numbers of expected background events are taken as systematic errors for that variable. The systematic errors for the LH selection are estimated in a similar way. The total systematic errors due to the modelling of the selection variables including those entering the LH selection are calculated by summing the errors in quadrature for each category at each \sqrt{s} individually. The evaluated errors are summarised in Table 5. The statistical errors due to the finite size of the MC samples and the uncertainty on the luminosity measurement are also estimated. The total systematic error ranges from 3.5% to 17.4% for the signal, and from 1.9% to 4.4% for the background.

Category		2-jet			>2-jet		
Decay Mode		Inv.	Nearly Inv.		Inv.	Nearly Inv.	
ΔM (GeV)		—	2	4	—	2	4
Selection variable	Signal	0.2-3.9%	0.0-5.0%	0.0-11.1%	0.3-4.1%	0.4-4.7%	0.6-10.3%
	BKG	0.7-2.2%			1.0-1.9%		
MC statistics	Signal	3.3-7.3%	5.2-10.9%	6.5-15.4%	3.6-8.8%	5.0-9.5%	4.8-11.0%
	BKG	1.9-3.8%			1.4-2.7%		
Luminosity		0.5%					
Total	Signal	3.5-7.8%	5.3-10.7%	5.8-17.4%	3.7-9.5%	5.1-7.8%	4.8-11.4%
	BKG	2.2-4.4%			1.9-3.4%		

Table 5: *Ranges of estimated relative systematic errors (in %) for all \sqrt{s} . Errors on the signal efficiency are estimated at each MC mass point at each \sqrt{s} and those for background at each \sqrt{s} . The total systematic error at each \sqrt{s} is calculated by summing the individual errors in quadrature.*

4 Results

Figure 4 shows the missing mass distribution for the selected candidate events together with the expected background and an expected signal of $m_{h^0} = 105$ GeV for the two categories, for all \sqrt{s} combined. No significant excess above the expected SM background is observed in either category. The main background comes from four-fermion processes in both categories. The broad peak around 70 GeV in the four-fermion histograms is due to the $e^+e^- \rightarrow W^+W^-$ process and the peak around 90 GeV is due to the $e^+e^- \rightarrow Z^0Z^0$ process. Final efficiencies are summarised in Table 3.

Limits are calculated using the likelihood ratio method described in Ref. [33]. The M_{miss} information is used as a discriminator in the calculation. Systematic errors on the background and signal estimate are taken into account.

4.1 Limits on the production of invisibly decaying Higgs bosons

Figure 5 (a) shows 95% confidence level (CL) limits on the production rate of an invisibly decaying Higgs boson relative to the predicted SM Higgs production rate, defined as

$$\text{BR}(h^0 \rightarrow \chi^0\chi^0) \frac{\sigma(e^+e^- \rightarrow Z^0h^0)}{\sigma(e^+e^- \rightarrow Z^0H_{\text{SM}}^0)} = \text{BR}(h^0 \rightarrow \chi^0\chi^0)R_\sigma$$

where $\sigma(e^+e^- \rightarrow Z^0h^0)$ and $\sigma(e^+e^- \rightarrow Z^0H_{\text{SM}}^0)$ are the production cross-sections of the invisibly decaying Higgs boson and the SM Higgs boson, respectively, and $\text{BR}(h^0 \rightarrow \chi^0\chi^0)$ is the branching ratio for the Higgs boson decay into a pair of invisible particles.

The observed and expected ratios shown in the figure are obtained from the results of this search, combined with LEP I data [13], and with results from the e^+e^- and $\mu^+\mu^-$ channels of the decay-mode independent searches [12]. For LEP I results, the recoil mass information is used as a discriminating variable, incorporated using a Gaussian mass resolution function; for the channels from the decay-mode independent search, the distribution of the squared recoil mass is used as a discriminant.

The full line in Figure 5 (a) represents the observed upper limit at 95% CL on the relative production rate as a function of the Higgs boson mass. A Higgs boson which couples to the Z^0 boson with SM strength and which decays exclusively into invisible final states is excluded up to a mass of 108.2 GeV at 95% CL assuming $\text{BR}(h^0 \rightarrow \chi^0\chi^0) = 100\%$, while a limit of 108.6 GeV is expected. The compatibility of the data with the expected background is quantified using the confidence (p -value) for background-only hypothesis, $1 - \text{CL}_b$ (see Ref. [3]) which is plotted in Figure 5 (b).

4.2 Limits on the production of nearly invisibly decaying Higgs bosons

The results obtained from two nearly invisible decay modes ($\chi^{0'} \rightarrow \chi^0 Z^*$ and $\chi^{0'} \rightarrow \chi^0 \gamma$) in this analysis are combined at each ΔM , where the lower of the two efficiencies is taken as the combined efficiency. The limit calculation uses only results from this analysis. In Figure 6 (a) and (b), limits on the production rate for a nearly invisibly decaying Higgs boson with $\Delta M = 2$ and 4 GeV are shown for the data taken between 183 GeV and 209 GeV. The production rate of the nearly invisibly decaying Higgs boson relative to the SM Higgs production rate is defined as

$$\text{BR}(h^0 \rightarrow \chi^0 \chi^{0'}) R_\sigma$$

where $\text{BR}(h^0 \rightarrow \chi^0 \chi^{0'})$ is the branching ratio for the decay into nearly invisible particles. The dependence of $1 - \text{CL}_b$ on the Higgs mass for nearly invisibly decaying Higgs bosons is shown in Figure 6 (c) and (d). A Higgs boson coupling to the Z^0 boson with SM strength and decaying into the nearly invisible final states is excluded up to a mass of 108.4 and 107.0 GeV at 95% CL for $\Delta M = 2$ and 4 GeV, respectively, assuming $\text{BR}(h^0 \rightarrow \chi^0 \chi^{0'}) = 100\%$. The corresponding expected limits are 108.2 and 107.3 GeV.

5 Conclusion

A search for invisibly decaying Higgs bosons has been performed using the data collected by the OPAL experiment at centre-of-mass energies between 183 and 209 GeV, corresponding to an integrated luminosity of 659.3 pb^{-1} . The search has not shown any excess over the expected background from SM processes. Limits on the production of invisibly decaying Higgs bosons were calculated combining the results with those from LEP I and those from e^+e^- and $\mu^+\mu^-$ channels of a decay-mode independent search at LEP II. Invisibly decaying Higgs bosons with masses below 108.2 GeV are excluded at 95% CL if they are produced with SM cross-sections, assuming $\text{BR}(h^0 \rightarrow \chi^0 \chi^0) = 100\%$. The search criteria were also applied to a search for nearly invisibly decaying Higgs bosons. Limits of 108.4 and 107.0 GeV were obtained for $\Delta M = m_{\chi^{0'}} - m_{\chi^0} = 2$ and 4 GeV, respectively.

Acknowledgements

We particularly wish to thank the SL Division for the efficient operation of the LEP accelerator at all energies and for their close cooperation with our experimental group. In addition to the support staff at our own institutions we are pleased to acknowledge the
Department of Energy, USA,
National Science Foundation, USA,
Particle Physics and Astronomy Research Council, UK,
Natural Sciences and Engineering Research Council, Canada,

Israel Science Foundation, administered by the Israel Academy of Science and Humanities,
Benozio Center for High Energy Physics,
Japanese Ministry of Education, Culture, Sports, Science and Technology (MEXT) and a grant
under the MEXT International Science Research Program,
Japanese Society for the Promotion of Science (JSPS),
German Israeli Bi-national Science Foundation (GIF),
Bundesministerium für Bildung und Forschung, Germany,
National Research Council of Canada,
Hungarian Foundation for Scientific Research, OTKA T-038240, and T-042864,
The NWO/NATO Fund for Scientific Research, the Netherlands.

References

- [1] P. W. Higgs, Phys. Lett. **B12** (1964) 132;
F. Englert and R. Brout, Phys. Rev. Lett. **13** (1964) 321;
G. S. Guralnik, C. R. Hagen, and T. W. B. Kibble, Phys. Rev. Lett. **13** (1964) 585.
- [2] S. L. Glashow, Nucl. Phys. **22** (1961) 579;
S. Weinberg, Phys. Rev. Lett. **19** (1967) 1264;
A. Salam, *Elementary Particle Theory*, ed. N. Svartholm (Almquist and Wiksells, Stockholm, 1968), 367.
- [3] The ALEPH, DELHI, L3 and OPAL Collaborations, The LEP working group for Higgs boson searches, Phys. Lett. **B565** (2003) 61.
- [4] H.P. Nilles, Phys. Rep. **110** (1984) 1;
H.E. Haber and G.L. Kane, Phys. Rep. **117** (1985) 75;
R. Barbieri *et al.*, Z. Physics at LEP1, CERN 89-08 (1989) Vol. 2, 121;
J.M. Frère, G.L. Kane, Nucl. Phys. **B223** (1983) 331;
J. Ellis *et al.*, Phys. Lett. **B123** (1983) 436;
J. Ellis *et al.*, Phys. Lett. **B127** (1983) 233.
- [5] K. Griest and H. E. Harber, Phys. Rev. **D37** (1988) 719;
A. Djouadi, P. Janot, J. Kalinowski and P. M. Zerwas, Phys. Lett. **B376** (1996) 220.
- [6] I. Antoniadis, M. Tuckmantel and F. Zwirner, Nucl. Phys. **B707** (2005) 215.
- [7] F. de Campos, O. J. Éboli, J. Rosiek and J. W. F. Valle, Phys. Rev. **D55** (1997) 1316;
Y. Chikashige, R. N. Mohapatra and P. D. Peccei, Phys. Lett. **B98** (1981) 265;
A. S. Joshipura and S. D. Rindani, Phys. Rev. Lett. **69** (1992) 3269.
- [8] S.P. Martin and J.D. Wells, Phys. Rev. **D60** (1999) 035006.
- [9] G.F. Giudice, R. Rattazzi and J.D. Wells, Nucl. Phys. **B595** (2001) 250.

- [10] T. Binoth and J.J. van der Bij, *Z. Phys.* **C75** (1997) 17.
- [11] The OPAL Collaboration, G. Abbiendi *et al.*, *Eur. Phys. J.* **C49** (2007) 457.
- [12] The OPAL Collaboration, G. Abbiendi *et al.*, *Eur. Phys. J.* **C27** (2003) 311.
- [13] The OPAL Collaboration, G. Alexander *et al.*, *Phys. Lett.* **B377** (1996) 273.
- [14] The OPAL Collaboration, G. Abbiendi *et al.*, *Eur. Phys. J.* **C35** (2004) 1.
- [15] The ALEPH Collaboration, A. Heister *et al.*, *Phys. Lett.* **B526** (2002) 191;
The DELPHI Collaboration, J. Abdallah *et al.*, *Eur. Phys. J.* **C32** (2004) 475;
The L3 Collaboration, P. Achard *et al.*, *Phys. Lett.* **B609** (2005) 35.
- [16] The OPAL Collaboration, K. Ahmet *et al.*, *Nucl. Instrum. Methods* **A305** (1991) 275 .
- [17] P. Janot, in *Physics at LEP2*, edited by G. Altarelli, T. Sjöstrand and F. Zwirner, CERN 96-01, vol. 2 (1996) 309.
- [18] T. Sjöstrand, *Comp. Phys. Comm.* **82** (1994) 74; id. **112** (1998) 227.
- [19] S. Jadach, B.F.L. Ward and Z. Wąs, *Comp. Phys. Comm.* **130** (2000) 260.
- [20] J. Fujimoto *et al.*, *Comp. Phys. Comm.* **100** (1997) 128.
- [21] M. Skrzypek *et al.*, *Comp. Phys. Comm.* **94** (1996) 216;
M. Skrzypek *et al.*, *Phys. Lett.* **B372** (1996) 289.
- [22] S. Jadach, W. Płaczek, B.F.L. Ward, *Phys. Lett.* **B390** (1997) 298.
- [23] D. Karlen, *Nucl. Phys.* **B289** (1987) 23.
- [24] S. Jadach, B. F. L. Ward, Z. Wąs, *Comp. Phys. Comm.* **79** (1994) 503.
- [25] E. Budinov *et al.*, in *Physics at LEP2*, edited by G. Altarelli, T. Sjöstrand and F. Zwirner, CERN 96-01, vol. 2 (1996) 216;
R. Engel and J. Ranft, *Phys. Rev.* **D54** (1996) 4244.
- [26] J.A.M. Vermaseren, *Nucl. Phys.* **B229** (1983) 347.
- [27] The OPAL Collaboration, G. Alexander *et al.*, *Z. Phys.* **C69** (1996) 543.
- [28] J. Allison *et al.*, *Nucl. Instrum. Methods* **A317** (1992) 47 .
- [29] The OPAL Collaboration, K. Ackerstaff *et al.*, *Eur. Phys. J.* **C2** (1998) 213.
- [30] The OPAL Collaboration, G. Alexander *et al.*, *Phys. Lett.* **B377** (1996) 181.
- [31] N. Brown and W. J. Stirling, *Phys. Lett.* **B252** (1990) 657;
S. Bethke, Z. Kunszt, D. Soper and W. J. Stirling, *Nucl. Phys.* **B370** (1992) 310;
S. Catani *et al.*, *Phys. Lett.* **B269** (1991) 432;
N. Brown and W. J. Stirling, *Z. Phys.* **C53** (1992) 629.

[32] The OPAL Collaboration, K. Ackerstaff *et al.*, Eur. Phys. J. **C1** (1998) 425.

[33] T. Junk, Nucl. Nucl. Instrum. Methods **A434** (1999) 435 .

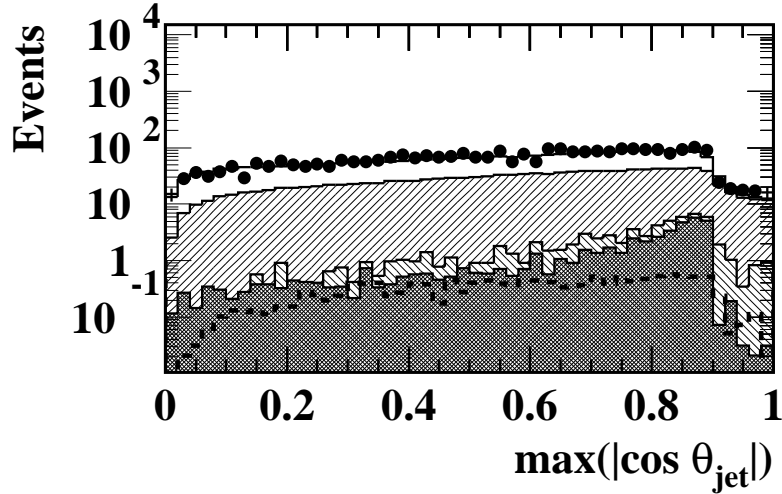
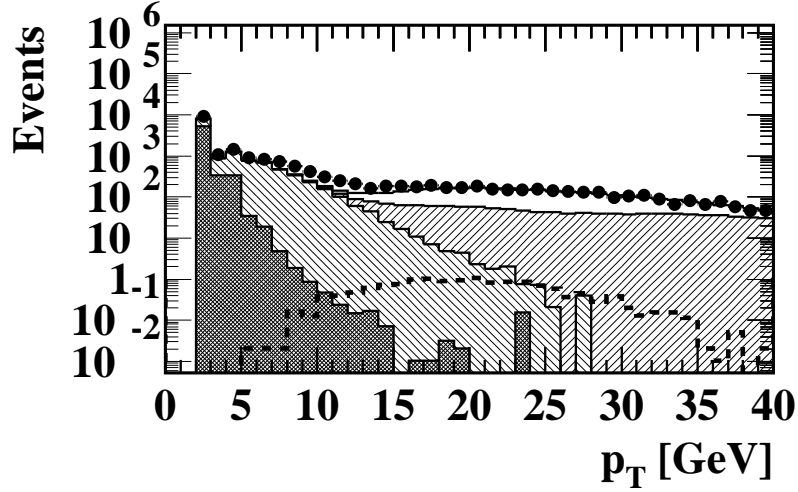


Figure 1: The distributions of p_T and $|\cos \theta_{\text{jet}}|$ at $\sqrt{s}=206$ GeV before applying the sequential cuts on the variables: data (dots with error bar) are shown together with the predicted contributions from the background processes; $e^+e^- \rightarrow \ell^+\ell^-$ (cross-hatched), two-photon processes (negative slope hatched), four-fermion processes (positive slope hatched), and $q\bar{q}(\gamma)$ (open). The background distributions have been normalised to 124.6 pb^{-1} . The distribution of simulated signals for the process $Z^0 h^0 \rightarrow (q\bar{q})(\chi^0 \chi^0)$ for $m_{h^0} = 105$ GeV are also shown with dashed line. The signal is normalised using the SM Higgs production cross-section and 100% production rate for the process $Z^0 h^0 \rightarrow (q\bar{q})(\chi^0 \chi^0)$.

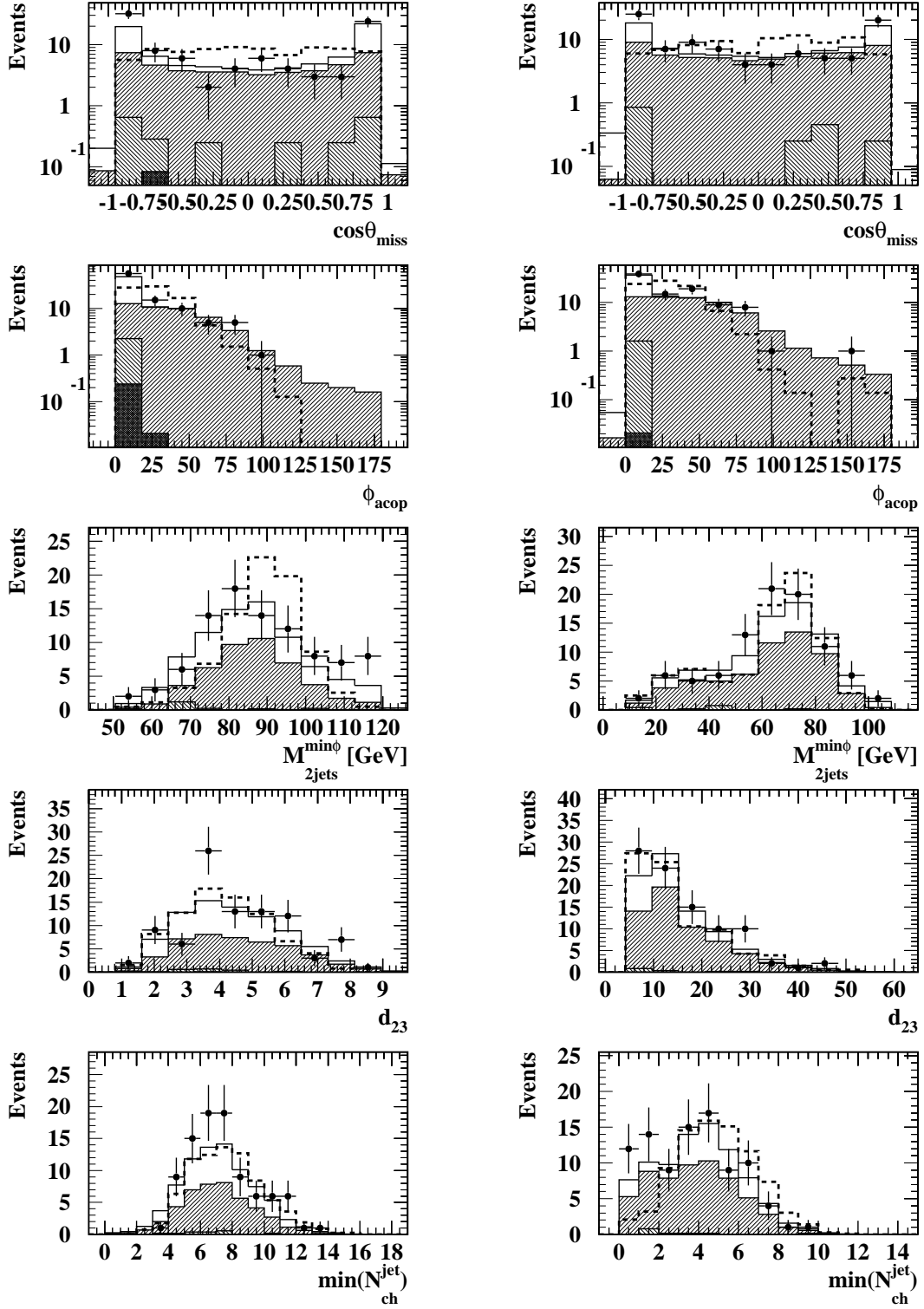


Figure 2: The distribution of likelihood input variables: $\cos\theta_{\text{miss}}$, ϕ_{acop} , $M_{2\text{jets}}^{\text{min}\phi}$, d_{23} and $\min(N_{\text{ch}}^{\text{jet}})$, at $\sqrt{s} = 206$ GeV for the 2-jet category (left) and the >2 -jet category (right). The background sources are shaded as in Figure 1. The distributions of the signal for simulated invisibly decaying Higgs bosons with $m_{\text{H}^0} = 105$ GeV are shown as dashed lines. The signal histograms are normalised to the number of events of the expected background. The first and last bins in each histogram include underflow and overflow, respectively.

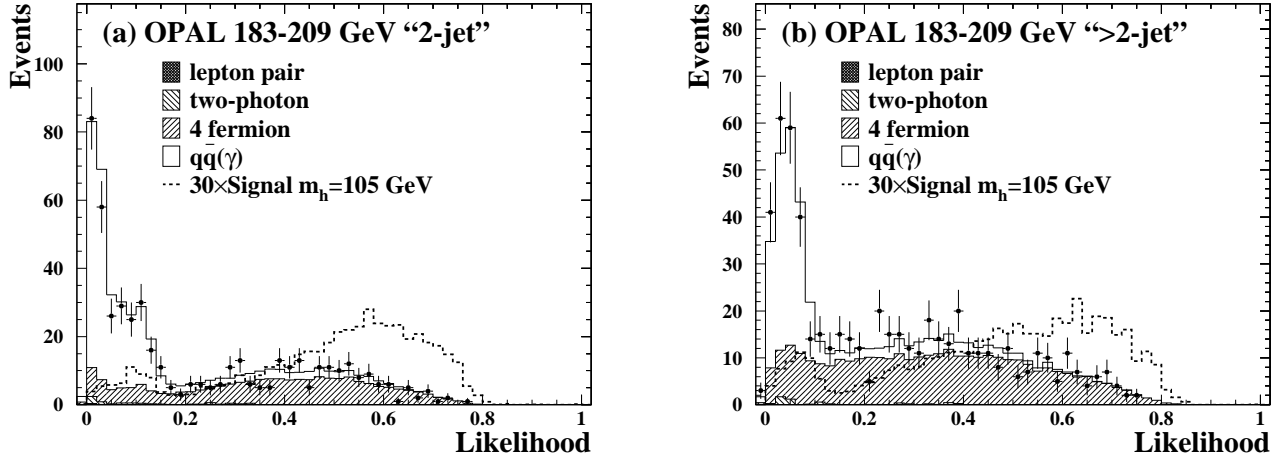


Figure 3: The distribution of likelihood output for $\sqrt{s}=183-209$ GeV for (a) the 2-jet category and (b) the >2-jet category. The background sources are shaded as in Figure 1. The distributions of the signal for simulated invisibly decaying Higgs bosons with $m_{h^0}=105$ GeV are also shown. The signal histograms are normalised using 30 times the production cross-section of the SM Higgs boson and 100% production rate for the process $Z^0 h^0 \rightarrow (q\bar{q})(\chi^0 \chi^0)$.

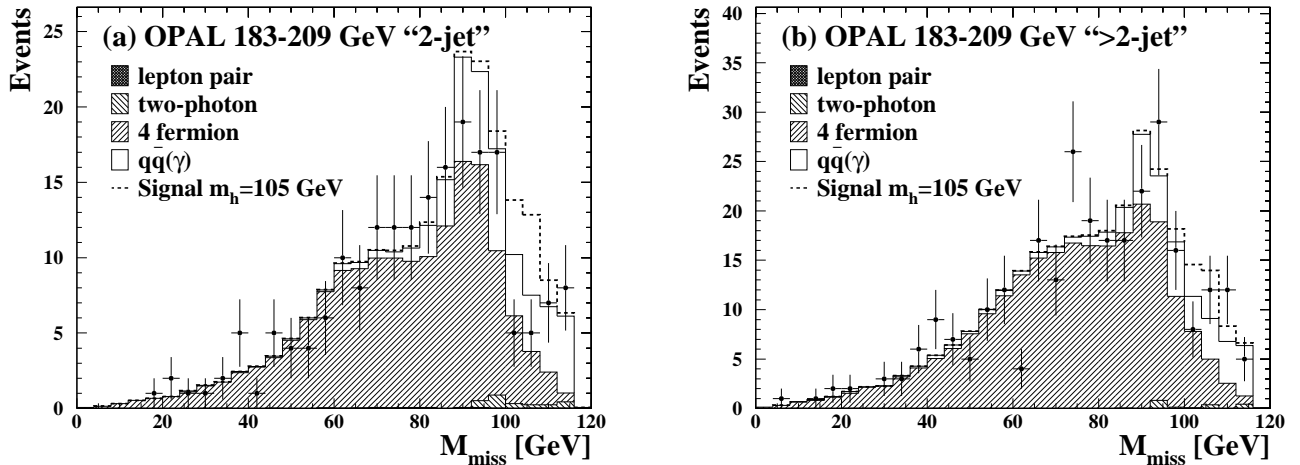


Figure 4: The distribution of missing mass for each category for all LEP2 data combined: (a) the 2-jet category and (b) the >2-jet category. The background sources are shaded as in Figure 1. The distributions of the signal for simulated invisibly decaying Higgs bosons with $m_{h^0}=105$ GeV are shown on top of the background distribution. The signal histograms are normalised using the production cross-section of the SM Higgs boson and 100% production rate for the process $Z^0 h^0 \rightarrow (q\bar{q})(\chi^0 \chi^0)$.

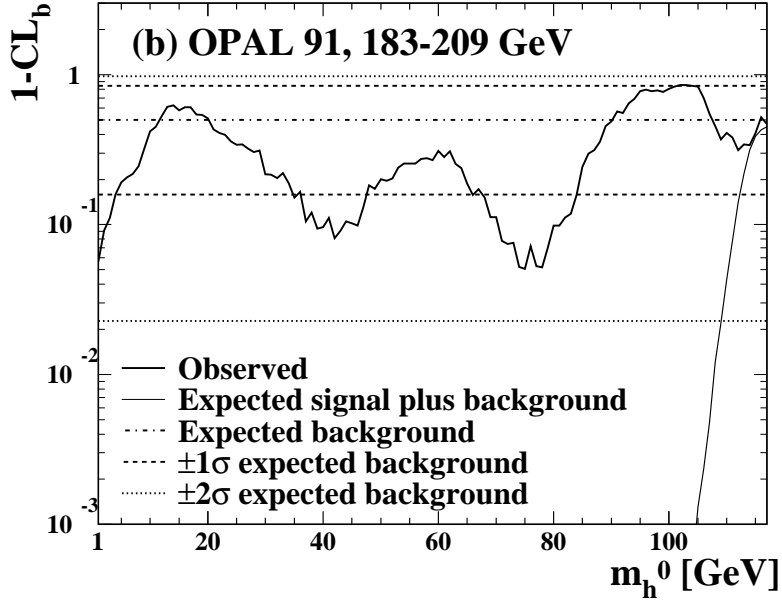
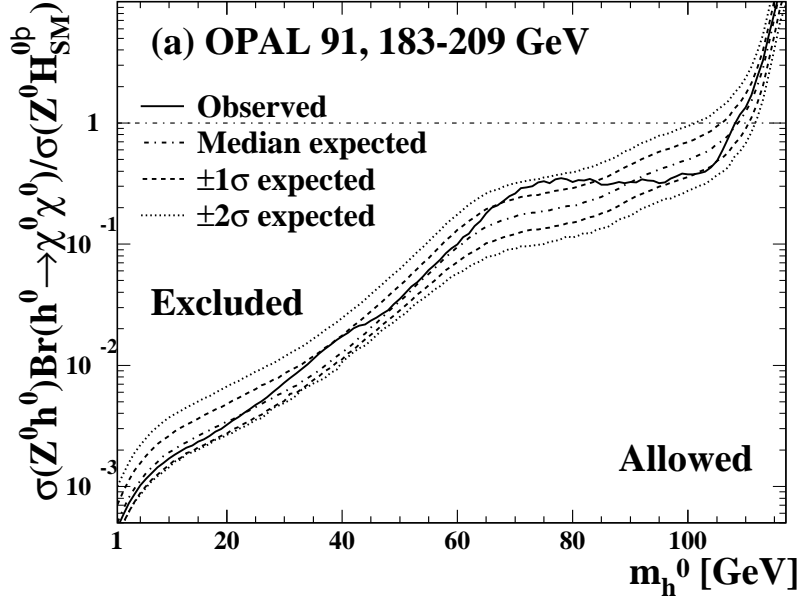


Figure 5: (a) Observed and expected limits on the relative production rate for $e^+e^- \rightarrow Z^0 h^0 \rightarrow Z^0 \chi^0 \chi^0$ (invisible decay) to the SM Higgs production rate at 95% CL as a function of the test mass m_{h^0} , assuming $\text{BR}(h^0 \rightarrow \chi^0 \chi^0) = 100\%$. The solid curves show the observed limits and the dot-dashed curves the median expected limits. The dashed and dotted curves show 1σ and 2σ bands of expected limits. (b) The background confidence $1 - \text{CL}_b$ as a function of m_{h^0} . The thick solid curve shows the observed $1 - \text{CL}_b$ and the thin solid curve the expectation in the signal plus background hypothesis. The dot-dashed, dashed and dotted lines show median $1 - \text{CL}_b$, and the 1σ and 2σ bands expected for the background only hypothesis, respectively.

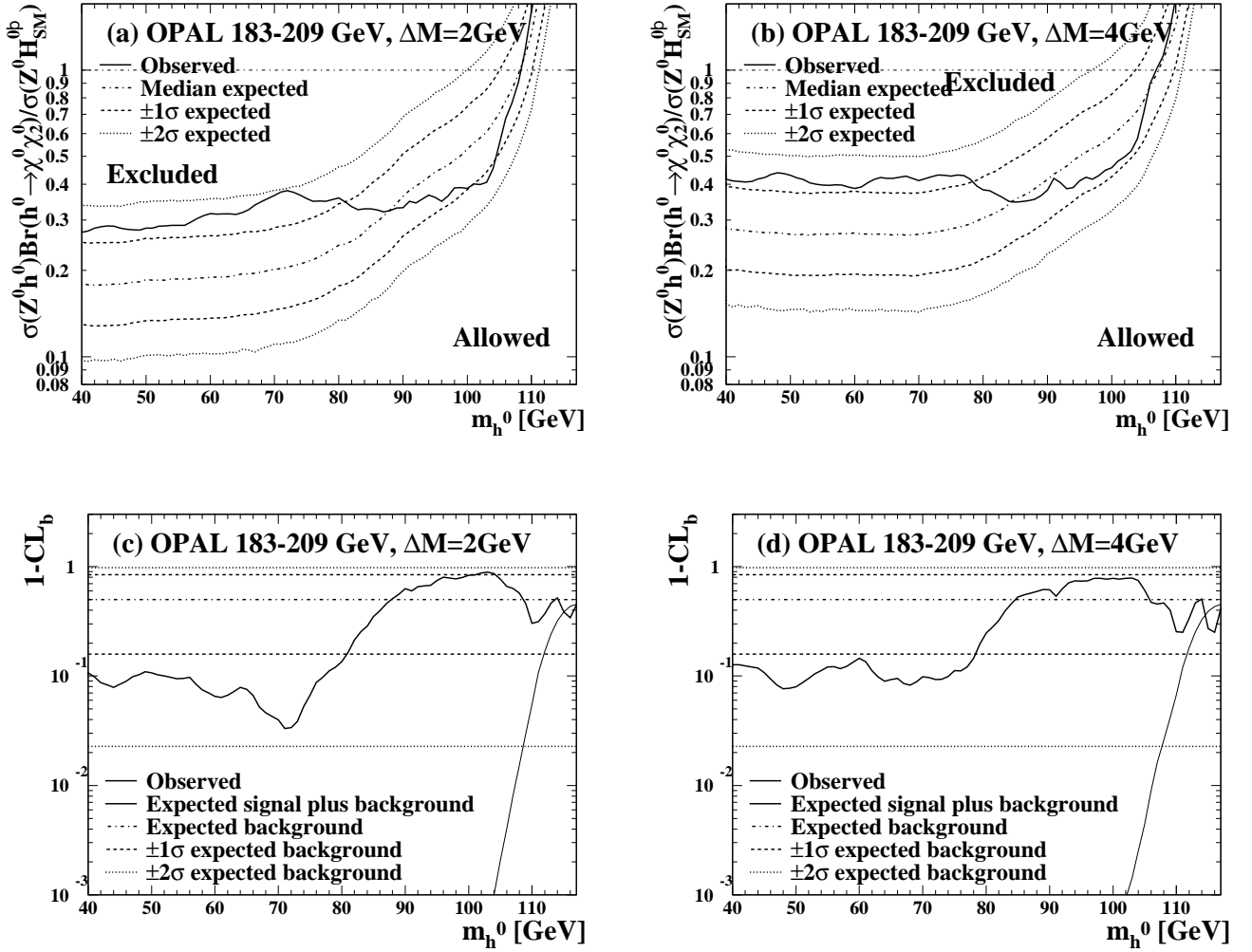


Figure 6: Limits on the relative production rate for $e^+e^- \rightarrow Z^0 h^0 \rightarrow Z^0 \chi^0 \chi^{0'}$ (nearly invisible decay) at the 95% CL, normalised to the SM production rate for $e^+e^- \rightarrow Z^0 H^0$, (a) for $\Delta M = 2$ GeV and (b) for $\Delta M = 4$ GeV, assuming $\text{BR}(h^0 \rightarrow \chi^0 \chi^{0'}) = 100\%$ as a function of m_{h^0} . Figure (c) and (d) show the $1 - \text{CL}_b$ for $\Delta M = 2$ and 4 GeV, respectively.